All-inorganic nitrate electrolyte for high-performance lithium oxygen battery

Dongyue Yang[1,2], Jiayi Du[1,2], Kai Chen[1], Haoran Zhang[1,2], Gang Huang[1,2], Tong Liu[1,2], Xinbo Zhang[1,2], and Hongjie Zhang[1,2] (✉)

[1] *State Key Laboratory of Rare Earth Resource Utilization, Changchun Institute of Applied Chemistry, Chinese Academy of Sciences, Changchun 130022, China*

[2] *School of Applied Chemistry and Engineering, University of Science and Technology of China, Hefei 230026, China*

ABSTRACT

Lithium-oxygen (Li-O_2) batteries have been regarded as an expectant successor for next-generation energy storage systems owing to their ultra-high theoretical energy density. However, the comprehensive properties of the commonly utilized organic salt electrolyte are still unsatisfactory, not to mention their expensive prices, which seriously hinders the practical production and application of Li-O_2 batteries. Herein, we have proposed a low-cost all-inorganic nitrate electrolyte (LiNO$_3$−KNO$_3$−DMSO) for Li-O_2 batteries. The inorganic nitrate electrolyte exhibits higher ionic conductivity and a wider electrochemical stability window than the organic salt electrolyte. The existence of K^+ can stabilize the O_2^- intermediate, promoting the discharge process through the solution pathway with an enlarged capacity. Even at an ultra-low concentration of 0.01 M, the K^+ can still remain stable to promote the solution discharge process and also possess a new function of inhibiting the dendrite growth by electrostatic shielding, further enhancing the battery stability and contributing to the long cycle lifetime. As a result, in the 0.99 M LiNO$_3$− 0.01 M KNO$_3$−DMSO electrolyte, the Li-O_2 batteries exhibit prolonged cycling performance (108 cycles) and excellent rate performance (2 A·g^{-1}), significantly superior to the organic salt one.

KEYWORDS

Li-O_2 batteries, potassium ions, inorganic nitrate electrolyte, solution pathway mechanism

1   Introduction

Given the surging demand for high-capacity energy storage systems (ESSs) in portable electronics and electric vehicles, numerous researchers are actively engaged in the development of highly efficient ESSs that surpass the energy density limitations of lithium-ion batteries (LIBs) [1, 2]. Nonaqueous Li-O_2 batteries exhibit an exceptionally high theoretical energy density of up to 3500 Wh·kg^{-1}, rendering them an ideal candidate for meeting the growing energy requirements of ESSs [3, 4]. In a typical Li-O_2 battery, O_2 undergoes reduction during discharge and forms solid Li$_2$O$_2$ discharge products, which are subsequently decomposed through reverse oxidation during charging [3, 5, 6]. At present, the development of Li-O_2 batteries is advancing by leaps and bounds. Nevertheless, there are still some issues and challenges that need to be addressed.

In terms of batteries, cost, capacity, and cycle stability are the three most critical parameters that largely determine their practicality [7–9]. The electrolyte, equivalent to the blood in the battery, plays an ion conduction role in the cell operation, which has a significant influence on the electrochemical performance, and directly determines the battery capacity and cycle stability [10, 11]. At present, Li-O_2 batteries commonly utilize organic salts to prepare the electrolytes, such as lithium bis(trifluoromethane)sulfonimide (LiTFSI) [12–15] and lithium

trifluoromethanesulphonate (LiOTf) [16]. Due to the complication of synthesis, the cost of these organic salts (¥25–45 g^{-1}) is significantly higher than that of inorganic ones (¥6–10 g^{-1}), such as LiPF$_6$ and LiNO$_3$ (Table S1 in the Electronic Supplementary Material (ESM)) [17, 18]. Furthermore, the anion of organic salt contains functional groups, such as C–F bond. The attack by superoxide radicals generated during discharge and charge processes would decompose these functional groups, which results in the formation of by-products (LiF and –CF$_3$) to passivate the cathode [19, 20]. Therefore, both in aspects of cost and stability, inorganic salt-based electrolytes are better choices to push Li-O_2 batteries one step further into a feasible technology.

Despite promising, most low-cost inorganic salts have been proven unstable in the Li-O_2 battery system. For instance, the most common LIBs salt (LiPF$_6$) [21, 22], would decompose to LiF, Li$_x$PF$_y$O$_z$, and other by-products during battery cycling [23, 24]. Moreover, in the presence of H$_2$O, the LiPF$_6$ could readily form HF to degrade the cell components [25]. In addition, other inorganic salts, like LiBF$_4$ and LiClO$_4$, are sensitive to the O_2-rich environments [24, 26]. By contrast, the inorganic nitrate (lithium nitrate, LiNO$_3$) exhibits better stability, and it is also a functional salt that can enlarge the discharge capacity of Li-O_2 batteries by increasing the solubility of LiO$_2$ intermediate in the electrolyte [27, 28]. Typically, the LiNO$_3$ is just employed as an electrolyte additive for increasing the discharge capacity in solvents with low donor

---

number (DN), such as tetraethylene glycol dimethyl ether (TEGDME), which might be owing to its poor solubility in the ether-based electrolytes [27]. The available NO_3^- in the electrolyte could act as a complexing agent to coordinate with the Li^+ to form soluble and stable complexes ($Li^+-NO_3^-$). Consequently, the increased stability of Li^+ in solution, in turn, induces enhanced solubility of the O_2^- intermediate to form large-sized Li_2O_2. This promotes the discharge process of $Li-O_2$ batteries through the conversion from surface pathway to solution pathway with an improved discharge capacity [29, 30]. However, for the solvent with high DN and high dielectric constant, like dimethyl sulfoxide (DMSO), although it has a good solubility to nitrate [31], the NO_3^- induced capacity increase no longer works. This can be ascribed to the well-solvation ability of the DMSO solvent to the Li^+, making NO_3^- have minimal impact on the Li^+ solvation process [30]. Therefore, if we could endow the $LiNO_3-DMSO$ electrolyte system with the ability to promote the solution discharge of $Li-O_2$ batteries and improve its compatibility with the Li metal anode, a low-cost high-performance inorganic electrolyte system would be hopefully developed.

To this end, we have designed a low-cost all-inorganic nitrate electrolyte ($LiNO_3-KNO_3-DMSO$) for $Li-O_2$ batteries. Compared with the organic salt electrolytes, the inorganic one developed here exhibits higher ionic conductivity and a wider electrochemical stability window. Moreover, attributing to the ability of K^+ to stabilize the O_2^- intermediate and its associated lowest energy barrier of disproportionation reaction to generate Li_2O_2, the introduction of K^+ can promote the discharge process through the solution pathway with an enlarged discharge capacity. Even at an ultra-low concentration of 0.01 M, this function of K^+ can still work well and also brings new benefit to protect the Li metal anode without dendrite growth, contributing to the long-cycle stability of the batteries. As a result, the $Li-O_2$ batteries with 0.99 M $LiNO_3$−0.01 M potassium nitrate (KNO_3)−DMSO electrolyte can stably operate for 234 and 108 cycles at 300 mA·g⁻¹ with limited capacities of 500 and 1000 mAh·g⁻¹, respectively, which are significantly superior to the battery with organic salt electrolytes.

2 Experimental

2.1 Materials

Superdry DMSO (99.7%, water ≤ 30 ppm) with molecular sieves was bought from J&K Scientific. $LiNO_3$ (99.99%), KNO_3 (99%), LiOTf (98%), TEGDME (99%), potassium superoxide (KO_2, 99.5%), N-methyl-2-pyrrolidinone (NMP), $RuCl_3 \cdot xH_2O$, and Pluronic F127 were purchased from Aladdin.

2.2 CNTs/Ru@CNTs (CNT = carbon nanotube) cathode preparation

CNTs/Ru@CNTs and polyvinylidene fluoride (PVDF) binder (mass ratio 4:1) were mixed in NMP solvent. The obtained slurry was sprayed on the carbon paper and then dried in a vacuum oven at 80 °C. The final loading mass was controlled at 0.3 mg·cm⁻². It was worth mentioning that the Ru@CNTs cathodes were only employed for testing the cycle performance of $Li-O_2$ batteries, and its synthesis method was based on the work we reported earlier [32].

2.3 Battery assembly

CR2025 coin cells with holes (cathode side) were used to assemble $Li-O_2$ batteries, which consisted of a lithium metal anode (φ14 mm), an air cathode (φ12 mm), and a glass fiber separator. The electrolyte used here was 100 μL x M $LiNO_3−y$ M KNO_3−DMSO ($x + y = 1$). After that, the assembled cells were rested in the bottles full of pure O_2 for 4 h before the electrochemical test. The symmetrical Li/Li cells were assembled by two lithium sheets separated by a glass fiber separator with 70 μL electrolyte.

2.4 Characterization

Battery discharging and charging test was carried out on a LAND (CT2100A). Scanning electron microscopy (SEM) test was conducted on a S-4800 field emission scanning electron microscopy. Powder X-ray diffraction (XRD) test was performed on a Bruker D8 Focus powder X-ray diffractometer. X-ray photoelectron spectroscopy (XPS) analysis was conducted on an ESCALAB MK II X-ray photoelectron spectrometer. Electrochemical impedance spectroscopy (EIS) and linear sweep voltammetry (LSV) tests were measured by a BioLogic VMP3 electrochemical workstation. *In-situ* pressure monitor test was carried out according to the method we previously reported [33]. Inductively coupled-optical emission spectroscopy (ICP-OES) was conducted on a TJA (Thermo Jarrell Ash) Atomscan Advantage instrument.

2.5 Density function theory (DFT) calculations

The Gaussian 16 software package was employed for all calculations [34]. Implicit solvation models were built by adding DMSO molecules one by one until the energy of coordination between target monomer/dimer and DMSO molecules reached the maximum value. Then, these molecule structures were optimized at the level of B3LYP-D3(BJ)/6-311G+(d) without negative frequency and thermal corrections, and the Gibbs Free
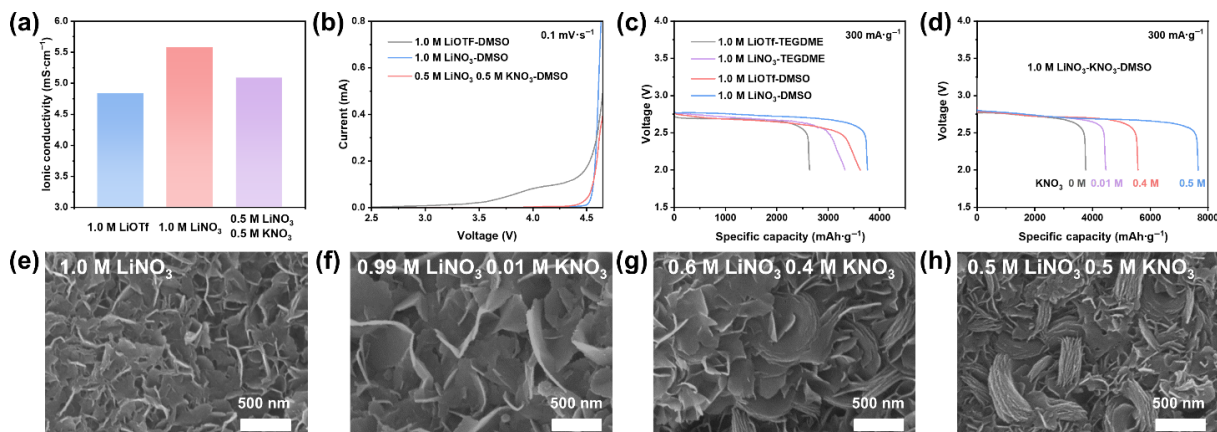
Figure 1 (a) Ionic conductivity and (b) LSV curves of organic salt and inorganic nitrate-based electrolytes. (c) Full discharge curves of $Li-O_2$ batteries with different electrolytes. (d) Discharge capacity of $Li-O_2$ cells with 1.0 M $LiNO_3-KNO_3$−DMSO electrolyte. SEM images of the CNTs cathodes after discharge at 1000 mAh·g⁻¹ and 300 mA·g⁻¹ in (e) 1.0 M $LiNO_3$, (f) 0.99 M $LiNO_3$−0.01 M KNO_3, (g) 0.6 M $LiNO_3$−0.4 M KNO_3, and (h) 0.5 M $LiNO_3$−0.5 M KNO_3.

Energy was simultaneously obtained [35–37]. The B2PLYP-D3(BJ)/def2-TZVP was used to perform high accurate single-point energy calculations. The solvent effects were conducted at the level of M06-2X-D3/6-31G+(d) with the solvation model of SMD [38].

3 Results and discussion

As presented in Fig. 1(a), the ionic conductivity of 1.0 M $LiNO_3$ electrolyte is 5.58 mS·cm^{-1}, which is higher than that of 1.0 M LiOTf electrolyte (4.84 mS·cm^{-1}). In addition, the 1.0 M $LiNO_3$ electrolyte also exhibits high voltage stability close to 4.5 V, while the 1.0 M LiOTf electrolyte begins to decompose when the voltage exceeds 4.0 V (Fig. 1(b)). Except for oxidation stability, the reduction stability of the electrolytes was also investigated. As presented in Fig. S1 in the ESM, compared with the 1.0 M LiOTf electrolyte, the 1.0 M $LiNO_3$ electrolyte shows a higher onset reduction potential with a large response current, which indicates that the inorganic nitrate electrolyte is more prone to be reduced and consequently facilitates the formation of a protective film on the Li metal anode [39]. Therefore, the inorganic nitrate electrolyte has faster ion conduction, higher voltage stability, and better film-formation ability, which are more conducive to the battery's long-term operation. Furthermore, the introduction of K$^+$ does not significantly sacrifice the ionic conductivity, electrochemical window, and reduction stability of the electrolytes (Figs. S1–S3 in the ESM). After confirming the advantages of the inorganic nitrate electrolytes, the capacities of Li-O_2 batteries with different electrolytes were checked. For the battery with $LiNO_3$–TEGDME-based electrolyte (low DN), it delivers higher capacity than the battery with LiOTf salt. However, in DMSO-based electrolyte (high DN), the $LiNO_3$ has little effect on promoting the battery capacity due to the superior solvation ability of DMSO towards the Li$^+$ (Fig. 1(c)), consistent with the previously reported results [30]. Unexpectedly, the introduction of K$^+$ to DMSO–NO$_3^-$ electrolyte could increase the cell capacity (Fig. 1(d)). In the pure Li$^+$ electrolyte, the discharge capacity of the Li-O_2 battery is 3460 mAh·g^{-1} at 300 mA·g^{-1}. The battery capacity enlarges as the K$^+$ concentration in the electrolyte increases. In the 0.5 M $LiNO_3$–

0.5 M KNO_3 electrolyte, the capacity reaches 7656 mAh·g^{-1} at the same circumstance, certifying the function of K$^+$ to promote the capacity increase.

The CNTs cathodes after discharge at 1000 mAh·g^{-1} in different electrolytes were then characterized by scanning electron microscopy (SEM, Figs. 1(e)–1(h)). It can be seen that some sheet-like discharge products form on the CNTs cathode in the 0.99 M $LiNO_3$–0.01 M KNO_3 electrolyte (Fig. 1(f)), which are obviously larger than the sheets in 1.0 M $LiNO_3$ (Fig. 1(e)). Moreover, as the concentration of K$^+$ increases, the sheet-like discharge products accumulate and transform into toroid-like structures (Figs. 1(g) and 1(h)). The enlarged toroidal discharge products in 0.5 M $LiNO_3$–0.5 M KNO_3 electrolyte correspond to its high discharge capacity. As well, the SEM images of the discharge products after full discharge with four kinds of electrolyte are presented in Fig. S4 in the ESM, which exhibits a similar phenomenon to the above results.

As we all know, the main discharge products of K-O_2 batteries are KO_2 [40]. To verify whether the presence of K$^+$ in Li-O_2 battery affects the composition of the discharge product (Li_2O_2), X-ray diffraction (XRD) and X-ray photoelectron spectroscopy (XPS) characterizations were conducted. As presented in Fig. 2(a), the peaks at 2θ = 32.9°, 35.01°, and 58.68° can be attributed to the Li_2O_2. No by-products form on the CNTs cathodes, and all discharge products decompose after the subsequent re-charge process (Fig. S5(a) in the ESM). Interestingly, although in the 1.0 M KNO_3 electrolyte, the discharge product remains Li_2O_2 rather than KO_2. This can be further demonstrated by the XPS characterization (Figs. S5(b)–S5(d) in the ESM). The absence of the N 1s signal indicates that the salt on the cathodes has been cleaned up (Figs. S5(c) and S5(d) in the ESM). Therefore, the obtained information pertains solely to the discharge products deposited on the CNTs cathodes. Figures 2(b) and 2(c) show the O 1s and Li 1s spectra of the CNTs cathodes after discharge at 300 mA·g^{-1} and 1000 mAh·g^{-1}, respectively. The O 1s and Li 1s peaks at ~ 531.6 and ~ 55.0 eV are consistent with the previously reported XPS studies for confirming the Li_2O_2 formation in Li-O_2 cells [41, 42]. Importantly, as the concentration of K$^+$ increases, there are no noticeable variations in both O 1s and Li 1s spectra,
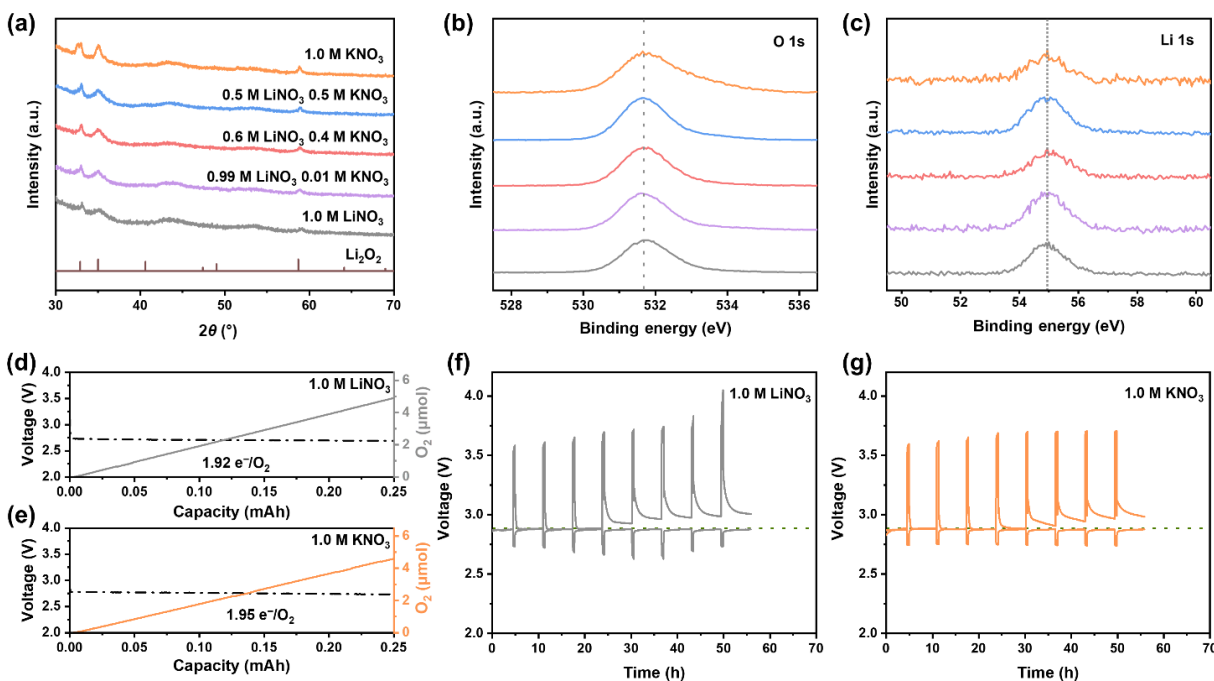
Figure 2 (a) XRD patterns of the CNTs cathodes after discharge in different electrolytes. (b) O 1s and (c) Li 1s XPS spectra of the discharged cathodes. *In-situ* pressure monitoring during discharge of Li-O_2 batteries in (d) 1.0 M $LiNO_3$ and (e) 1.0 M KNO_3. GITT curves of Li-O_2 batteries in (f) 1.0 M $LiNO_3$ and (g) 1.0 M KNO_3.

indicating that the Li_2O_2 discharge products remain unchanged regardless of the K^+ concentration. In addition, the undetected K peaks in the spectra of K 2p (Fig. S5(b) in the ESM) further verify the absence of K in the discharge products. The above results clearly attest that the introduction of K^+ in the DMSO–NO_3^- electrolyte could increase the discharge capacity without changing the typical Li-O_2 electrochemistry with the formation and decomposition of Li_2O_2.

So why the discharge product is Li_2O_2 instead of KO_2 even in the 1.0 M KNO_3–DMSO electrolyte? According to the Nernst Equation, when the concentration ratio of Li^+ to K^+ is higher than a small value (9.141×10^{-7}, Section S1 in the ESM), the Li_2O_2 would be the only final discharge product generated on the cathode surface. This can be ascribed to the chemical reaction between the intermediate KO_2 and Li^+. To further confirm the above spontaneous reaction, the 1.0 M $LiNO_3$–DMSO solution (5 mL) was dropwise added to the 3 mmol light yellow KO_2 powders. As presented in Fig. S6 in the ESM, during the dripping process, gas evolution and precipitation of white powders can be observed, which is attributed to the well-known disproportionation reaction $2KO_2 + 2Li^+ = Li_2O_2 + 2K^+ + O_2$ [43]. Therefore, the K^+ could act as a mediator during the discharge process without changing the final product of the Li-O_2 battery. To further prove this, *in-situ* pressure monitor and galvanostatic intermittent titration technique (GITT) test were conducted. Figures 2(d) and 2(e) display the oxygen consumption profiles of Li-O_2 batteries with 1.0 M $LiNO_3$ and 1.0 M KNO_3, respectively. The pressure variations during discharge indicate that the nearly two-electron transfer corresponding to the Li_2O_2 formation is followed in both electrolytes, signifying that the 1.0 M KNO_3 does not alter the discharge process. For the GITT curves of Li-O_2 batteries using 1.0 M $LiNO_3$ or KNO_3, both of them show an equilibrium potential near 2.87 V vs. Li^+/Li (Figs. 2(f) and 2(g)), which is consistent with the thermodynamic voltage value (2.96 V) for the governing reaction of $2Li^+ + 2e^- + O_2 = Li_2O_2$.

The detailed functions of K^+ played in the discharge process can be described as follows. During discharge, the O_2 absorbed on the cathode side first obtains one electron to generate O_2^-. According to the Soft–Hard–Acid–Base theory, the weaker acidity of K^+ compared with the Li^+ is inclined to stabilize O_2^- with weak alkalinity [44]; so in the hybrid electrolyte, the K^+ can promote the solution discharge pathway and accordingly increase the discharge

capacity without changing the composition of the discharge product. DFT calculations were then employed to obtain a profound understanding of the superoxide disproportionation reaction during the discharge process in the hybrid electrolyte system (M = Li, K) [45]. Firstly, the formation energy of KO_2 (−2.08 eV) is lower than that of LiO_2 (−1.93 eV), indicating that the O_2^- is more likely to bind to K^+ (Fig. 3(a)). Moreover, as presented in Fig. 3(b) and Table S2 in the ESM, the LiO_2 also shows higher energy than the KO_2. In the bare Li^+ electrolyte, the LiO_2 exhibits a small energy barrier of 0.21 eV to form the dimer of $Li_2(O_2)_2$ followed by downhill O_2 release and Li_2O_2 precipitation. While in the bare K^+ electrolyte, the energy barrier from KO_2 to $K_2(O_2)_2$ (2.19 eV) is too high to occur. By contrast, in the Li^+/K^+ hybrid electrolyte, the K^+ preferentially binds to O_2^-, and then Li^+ combines with KO_2 to form $LiK(O_2)_2$ dimers with an almost negligible energy barrier (0.01 eV). It is clear that $LiKO_4$ possesses a much lower energy barrier (−2.64 eV) for the disproportionation reaction to generate $LiKO_2$ and O_2 and continues to go downhill to generate the Li_2O_2 final discharge product. Among the above three possible reaction paths, the discharge process through the $LiK(O_2)_2$ dimers always exhibits the lowest energy barriers. This indicates that the introduction of K^+ could behave as a mediator to reduce the energy barrier of the disproportionation reaction in the discharge process, making Li_2O_2 easier to be generated in the hybrid electrolyte system.

Then, the question comes whether the K^+ still has the above effects with a small concentration. To confirm this, the variation of the content of Li^+ and K^+ in the 0.99 M $LiNO_3$–0.01 M KNO_3 electrolyte and on the cathodes was recorded by the inductively coupled plasma (ICP) spectrometry after different discharge time. As presented in Fig. 3(d), the concentrations of Li^+ and K^+ in the electrolyte remain almost constant during the continuous discharge process. For the cathodes, the Li^+ content gradually increases as the discharge time increases, while there is almost no K^+ (Fig. 3(e)). Moreover, the practical yield of Li_2O_2 is close to the theoretical value (Section S2 in the ESM), signifying that the addition of K^+ would not change the composition of the discharge product (Li_2O_2). Therefore, even at an ultra-low concentration of 0.01 M, there is still always available K^+ existing in the electrolyte to ensure that the discharge process of the Li-O_2 batteries is dominated by the solution pathway with enlarged capacity (Fig. 3(f)).
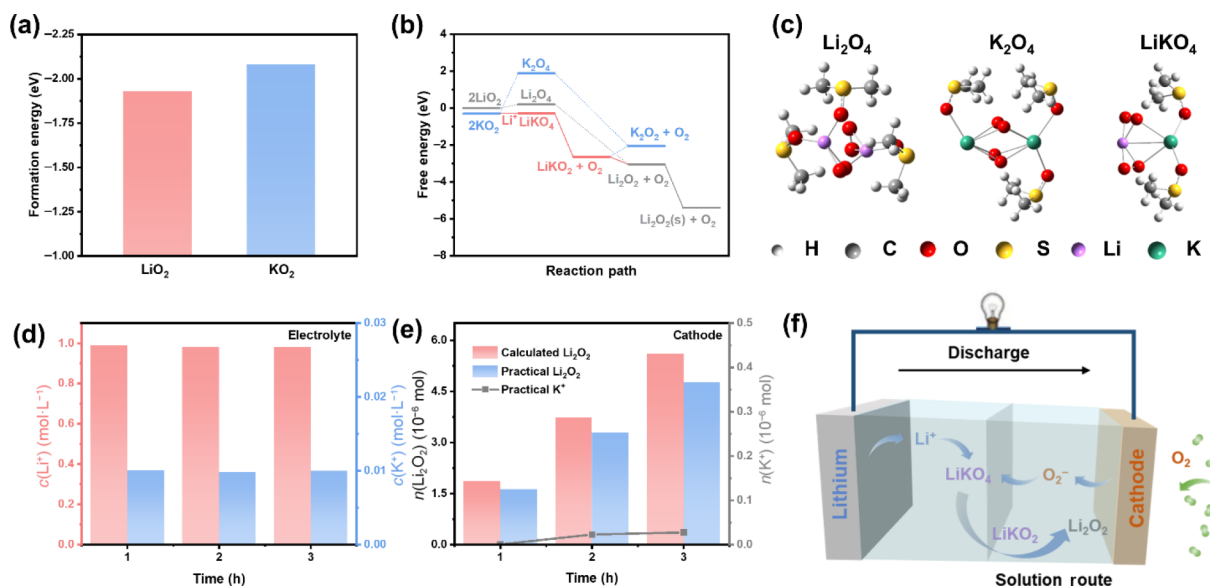

Figure 3 (a) Formation energies of LiO_2 and KO_2. (b) Reaction free energy profiles for superoxide disproportionation with various cations. (c) Solvation structures of Li_2O_4, K_2O_4, and $LiKO_4$. Variation of Li^+ and K^+ content (d) in the electrolyte and (e) on the cathode during discharge process. (f) Schematic of a Li-O_2 cell with K^+-containing electrolyte during the discharge process.

Besides the cathode side, it is noteworthy that the 0.01 M K⁺ in the hybrid electrolyte also exhibits a lower reduction potential compared to the Li⁺ (Table S4 in the ESM). This characteristic could enable K⁺ to effectively safeguard the lithium metal anode against dendrite growth through the self-healing electrostatic shield [46, 47]. The small amount of positively charged K⁺ would aggregate around the initially formed protruded Li, creating an electrostatic shield. Consequently, the Li⁺ tends to preferentially deposit in the neighboring regions of the protrusions, mitigating the dendrite growth by virtue of the repulsive force exerted by K⁺ (Fig. 4(a)). After this, Li/Li symmetrical batteries were assembled to prove the anode protection effect of the K⁺. As presented in Fig. 4(b), the results show that the Li/Li symmetrical battery with 1.0 M LiNO₃ experiences a sudden voltage decrease (the sign of short-circuit) just after cycling for 550 h. The SEM images of the Li deposition morphology in 1.0 M LiNO₃ after 45 and 100 cycles are presented in Figs. 4(c) and 4(d), respectively. It can be observed that serious dendrites and cracks emerge on the surface of the cycled Li anodes. On the contrary, for the symmetrical cell with 0.99 M LiNO₃–0.01 M KNO₃, it exhibits low discharge-charge voltages and long cycling life for over 1000 h, and the cycled Li anodes possess smooth surfaces without observable dendrite growth (Figs. 4(e) and 4(f)). Additionally, the impedance of the cell with 1.0 M LiNO₃ displays a continuous increase during cycling, whereas the impedance of the cell with 0.99 M LiNO₃–0.01 M KNO₃ remains relatively constant (Fig. S7 in the ESM), aligning with the observed overpotential changes for symmetrical cells. These results clearly prove that the small amount of K⁺ can protect the Li anode with a prolonged lifetime.

Since the confirmation of the advantages of the 0.99 M LiNO₃–0.01 M KNO₃ nitrate-based electrolyte itself and its positive effects on both the cathode and anode sides, the practical application ability of this electrolyte was checked in real Li-O₂ batteries. As expected, the battery in 0.99 M LiNO₃–0.01 M KNO₃

electrolyte could realize long cycle lives of 234 and 108 cycles at 300 mA·g⁻¹ with limited capacities of 500 mAh·g⁻¹ (Fig. 5(a) and Fig. S8 in the ESM) and 1000 mAh·g⁻¹ (Fig. 5(b) and 5(c)), respectively, much longer than those of the batteries with 1.0 M LiNO₃. When the concentration of KNO₃ increases, the cycling life of Li-O₂ cells decreases to some extent (Figs. S9 and S10 in the ESM). As presented in Fig. S10 in the ESM, in the 0.9 M LiNO₃–0.1 M KNO₃ electrolyte, the battery can operate for 106 cycles at 300 mA·g⁻¹ and 1000 mAh·g⁻¹. Further increasing the KNO₃ concentration to 0.4 and 0.5 M, the cells' lifetime decreases to 90 and 80 cycles, respectively, which are still higher than the cell with 1.0 M LiNO₃ electrolyte (60 cycles, Fig. 5(d)). The K⁺ concentration increase induced decline of battery cycle life is mainly because that the vanishment of the anode protection effect and the deposition of potassium (Table S4 in the ESM) rendered decomposition of the DMSO solvent during cycling [48]. It is also worth mentioning that the cycle life of the battery in 1.0 M LiNO₃ electrolyte is longer than that of the battery in 1.0 M LiOTf electrolyte (60 vs. 41 cycles, Fig. S11 in the ESM), highlighting the beneficial effects of the inorganic nitrate in extending the battery lifetime.

Considering that the high ionic conductivity of the inorganic nitrate electrolyte could improve the mass transfer kinetics, the rate capability of Li-O₂ batteries with different electrolytes was checked. In the process of constant change of current density for every 200 mAh·g⁻¹, the cell in 1.0 M LiOTF electrolyte shows a significant drop in voltage platform at 1000 mA·g⁻¹, while the cell in 1.0 M LiNO₃ electrolyte still exhibits a stable discharge profile with low overpotential (Fig. S12 in the ESM). Moreover, due to the stable and fast combination ability of K⁺ towards the O₂⁻ in the electrolyte [40, 45], the batteries with K⁺-containing electrolytes display stable voltage plateaus near 2.75 V even at a high current density of 2000 mA·g⁻¹ (Fig. 5(e)). These results verify that the optimized 0.99 M LiNO₃–0.01 M KNO₃–DMSO electrolyte
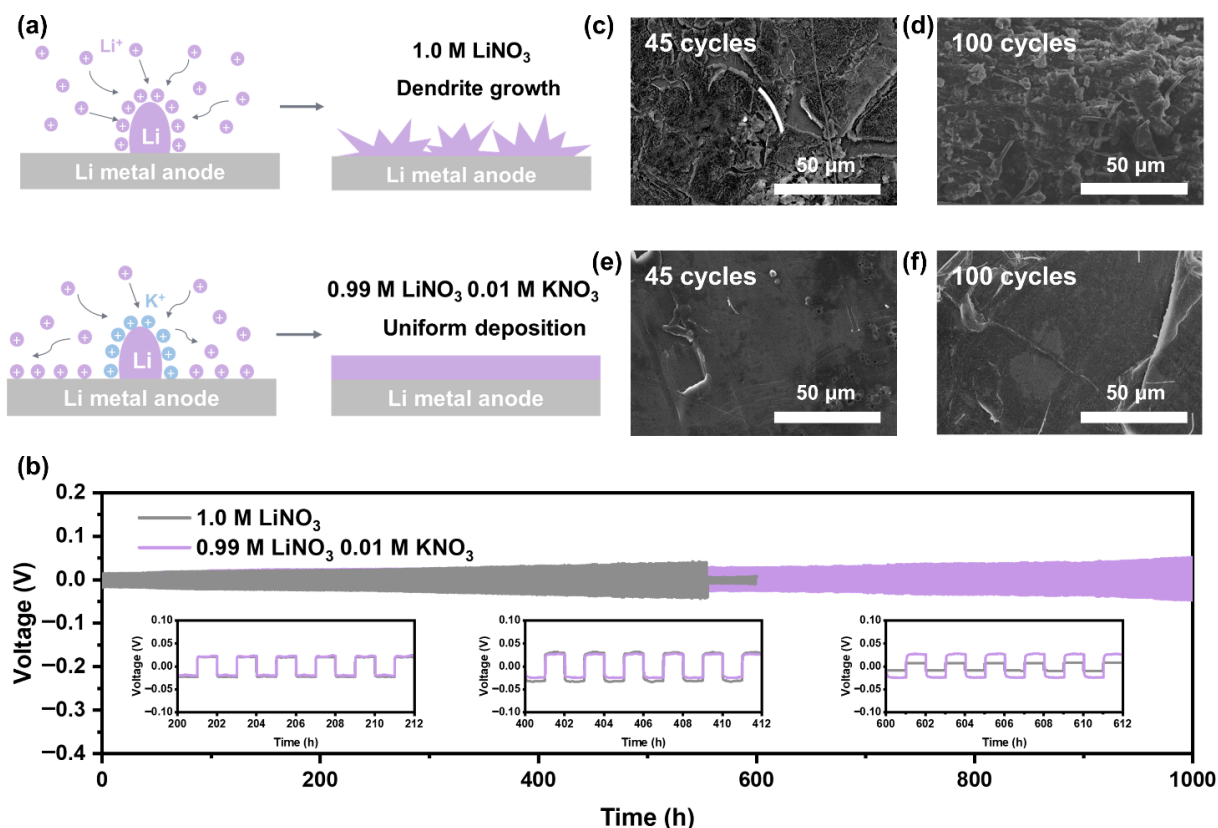
Figure 4 (a) Schematic diagram of Li⁺ deposition in two different electrolytes. (b) Cycling performance of Li/Li symmetrical cells at 0.1 mA·cm⁻² and 0.1 mAh·cm⁻². Inset figures are the representative voltage–time amplification curves. SEM images of the Li morphology in 1.0 M LiNO₃ after (c) 45 cycles and (d) 100 cycles. SEM images of the Li morphology in 0.99 M LiNO₃–0.01 M KNO₃ after (e) 45 cycles and (f) 100 cycles.
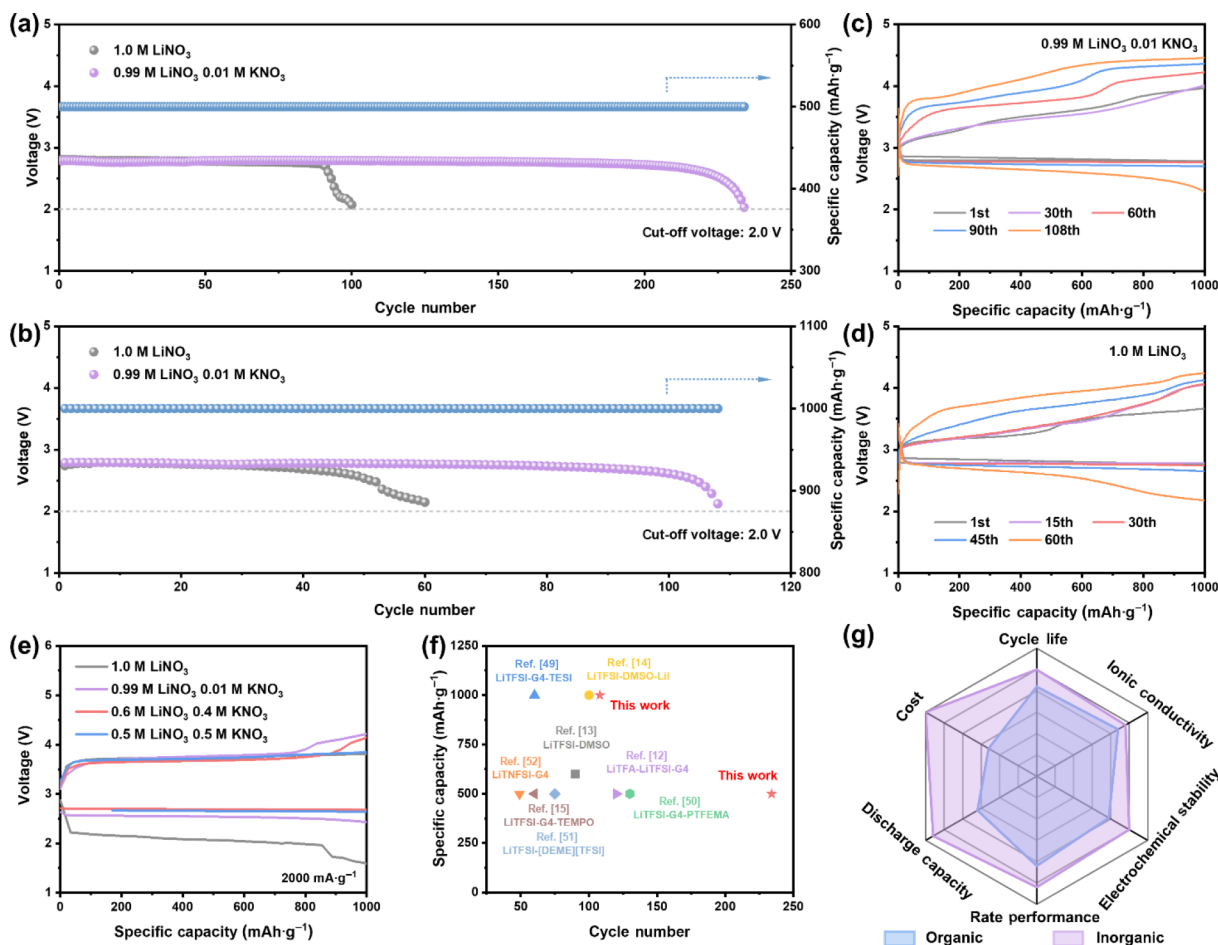
Figure 5 Cycling performance of Li-O₂ batteries with different electrolytes at 300 mA·g⁻¹ with a limited capacity of (a) 500 and (b) 1000 mAh·g⁻¹. The discharge cut-off voltage is 2.0 V. Discharge–charge profiles of Li-O₂ batteries with (c) 0.99 M LiNO₃–0.01 M KNO₃ and (d) 1.0 M LiNO₃. (e) Discharge–charge curves of Li-O₂ batteries at 2000 mA·g⁻¹. (f) Summarization of the cycle performances of Li-O₂ batteries with organic salt and inorganic nitrate-based electrolyte reported here. (g) Comparisons of the performances and properties of inorganic/organic electrolyte-based Li-O₂ batteries.

achieves excellent electrochemical performance in lifetime and rate capability, and especially, the lifetime achieved here is much superior to those of reported Li-O₂ batteries with organic salt-based electrolytes (Fig. 5(f)) [12–15, 49–52]. Consequently, the inorganic nitrate electrolyte developed here successfully reduces the electrolyte cost, accelerates the ion conduction, widens the electrochemical stability window, and brings positive effects on both the cathode and anode sides (Fig. 5(g)), making the high-capacity, long-cycle, and high-rate Li-O₂ batteries battery become possible.

4 Conclusions

In summary, we have developed a low-cost all-inorganic nitrate electrolyte (LiNO₃–KNO₃–DMSO) for Li-O₂ batteries. The designed electrolyte not only possesses higher ionic conductivity and wider electrochemical stability windows than the organic salt one but also could stabilize the O₂⁻ by the existing K⁺ to promote the battery to follow the solution discharge pathway with an enlarged discharge capacity. Especially, when decreasing the concentration of K⁺ to 0.01 M, the K⁺ could also safeguard the lithium metal anode against dendrite growth by the electrostatic shielding effect while maintaining the original function of facilitating the solution discharge process. As a result, the utilization of a 0.99 M LiNO₃–0.01 M KNO₃–DMSO electrolyte has enabled the successful development of high-capacity, long-cycle, and high-rate Li-O₂ batteries, thereby bringing this technology one step closer to practical implementation. This study presents a promising avenue for the design of advanced electrolytes for Li-O₂ batteries.

References

[1] Jiao, S. H.; Ren, X. D.; Cao, R. G.; Engelhard, M. H.; Liu, Y. Z.; Hu, D. H.; Mei, D. H.; Zheng, J. M.; Zhao, W. G.; Li, Q. Y. et al. Stable cycling of high-voltage lithium metal batteries in ether electrolytes. *Nat. Energy* **2018**, *3*, 739–746.

[2] Hou, B. W.; He, L.; Feng, X. N.; Zhang, W. F.; Wang, L.; He, X. M. Effect of amine additives on thermal runaway inhibition of SiC‖NCM811 batteries. *J. Electrochem.* **2023**, *29*, 2211141.

[3] Kwak, W. J.; Rosy; Sharon, D.; Xia, C.; Kim, H.; Johnson, L. R.; Bruce, P. G.; Nazar, L. F.; Sun, Y. K.; Frimer, A. A. et al. Lithium-oxygen batteries and related systems: Potential, status, and future. *Chem. Rev.* **2020**, *120*, 6626–6683.

[4] Cao, R. F.; Cui, Y. F.; Huang, G.; Liu, W. Q.; Liu, J. W.; Zhang, X.

B. Designing a photo-assisted Co-C$_3$N$_4$ cathode for high performance Li-O$_2$ batteries. *Nano Res.* **2023**, *16*, 8405–8410.

[5] Lu, J.; Li, L.; Park, J. B.; Sun, Y. K.; Wu, F.; Amine, K. Aprotic and aqueous Li-O$_2$ batteries. *Chem. Rev.* **2014**, *114*, 5611–5640.

[6] Chen, K.; Huang, G.; Zhang, X. B. Efforts towards practical and sustainable Li/Na-air batteries. *Chin. J. Chem.* **2021**, *39*, 32–42.

[7] Zheng, X. Y.; Huang, L. Q.; Ye, X. L.; Zhang, J. X.; Min, F. Y.; Luo, W.; Huang, Y. H. Critical effects of electrolyte recipes for Li and Na metal batteries. *Chem* **2021**, *7*, 2312–2346.

[8] Mauler, L.; Duffner, F.; Zeier, W. G.; Leker, J. Battery cost forecasting: A review of methods and results with an outlook to 2050. *Energy Environ. Sci.* **2021**, *14*, 4712–4739.

[9] Guo, R. Q.; Wu, F.; Wang, X. R.; Bai, Y.; Wu, C. Multi-electron reaction-boosted high energy density batteries: Material and system innovation. *J. Electrochem.* **2022**, *28*, 2219011.

[10] Ding, Z. Y.; Tang, Q. M.; Zhang, Q.; Yao, P. H.; Liu, X. J.; Wu, J. W. A flexible solid polymer electrolyte enabled with lithiated zeolite for high performance lithium battery. *Nano Res.* **2023**, *16*, 9443–9452.

[11] Xu, J. J.; Zhang, J. X.; Pollard, T. P.; Li, Q. D.; Tan, S.; Hou, S.; Wan, H. L.; Chen, F.; He, H. X.; Hu, E. Y. et al. Electrolyte design for Li-ion batteries under extreme operating conditions. *Nature* **2023**, *614*, 694–700.

[12] Cai, Y. C.; Hou, Y. P.; Lu, Y.; Zhang, Q.; Yan, Z. H.; Chen, J. Ionic liquid electrolyte with weak solvating molecule regulation for stable Li deposition in high-performance Li-O$_2$ batteries. *Angew. Chem., Int. Ed.* **2023**, *62*, e202218014.

[13] Liu, B.; Xu, W.; Yan, P. F.; Kim, S. T.; Engelhard, M. H.; Sun, X. L.; Mei, D. H.; Cho, J.; Wang, C. M.; Zhang, J. G. Stabilization of Li metal anode in DMSO-based electrolytes via optimization of salt-solvent coordination for Li-O$_2$ batteries. *Adv. Energy Mater.* **2017**, *7*, 1602605.

[14] Zhang, X. P.; Li, Y. N.; Sun, Y. Y.; Zhang, T. Inverting the triiodide formation reaction by the synergy between strong electrolyte solvation and cathode adsorption for lithium-oxygen batteries. *Angew. Chem., Int. Ed.* **2019**, *58*, 18394–18398.

[15] Ko, Y.; Park, H.; Lee, K.; Kim, S. J.; Park, H.; Bae, Y.; Kim, J.; Park, S. Y.; Kwon, J. E.; Kang, K. Anchored mediator enabling shuttle-free redox mediation in lithium-oxygen batteries. *Angew. Chem., Int. Ed.* **2020**, *59*, 5376–5380.

[16] Jung, H. G.; Hassoun, J.; Park, J. B.; Sun, Y. K.; Scrosati, B. An improved high-performance lithium-air battery. *Nat. Chem.* **2012**, *4*, 579–585.

[17] Ren, X. D.; Zou, L. F.; Cao, X.; Engelhard, M. H.; Liu, W.; Burton, S. D.; Lee, H.; Niu, C. J.; Matthews, B. E.; Zhu, Z. H. et al. Enabling high-voltage lithium-metal batteries under practical conditions. *Joule* **2019**, *3*, 1662–1676.

[18] Yu, Z. A.; Wang, H. S.; Kong, X.; Huang, W.; Tsao, Y.; Mackanic, D. G.; Wang, K. C.; Wang, X. C.; Huang, W. X.; Choudhury, S. et al. Molecular design for electrolyte solvents enabling energy-dense and long-cycling lithium metal batteries. *Nat. Energy* **2020**, *5*, 526–533.

[19] McCloskey, B. D.; Valery, A.; Luntz, A. C.; Gowda, S. R.; Wallraff, G. M.; Garcia, J. M.; Mori, T.; Krupp, L. E. Combining accurate O$_2$ and Li$_2$O$_2$ assays to separate discharge and charge stability limitations in nonaqueous Li-O$_2$ batteries. *J. Phys. Chem. Lett.* **2013**, *4*, 2989–2993.

[20] Veith, G. M.; Nanda, J.; Delmau, L. H.; Dudney, N. J. Influence of lithium salts on the discharge chemistry of Li-air cells. *J. Phys. Chem. Lett.* **2012**, *3*, 1242–1247.

[21] Freunberger, S. A.; Chen, Y. H.; Peng, Z. Q.; Griffin, J. M.; Hardwick, L. J.; Bardé, F.; Novák, P.; Bruce, P. G. Reactions in the rechargeable lithium-O$_2$ battery with alkyl carbonate electrolytes. *J. Am. Chem. Soc.* **2011**, *133*, 8040–8047.

[22] Ogasawara, T.; Débart, A.; Holzapfel, M.; Novák, P.; Bruce, P. G. Rechargeable Li$_2$O$_2$ electrode for lithium batteries. *J. Am. Chem. Soc.* **2006**, *128*, 1390–1393.

[23] Nasybulin, E.; Xu, W.; Engelhard, M. H.; Nie, Z. M.; Burton, S. D.; Cosimbescu, L.; Gross, M. E.; Zhang, J. G. Effects of electrolyte salts on the performance of Li-O$_2$ batteries. *J. Phys. Chem. C* **2013**, *117*, 2635–2645.

[24] Younesi, R.; Urbonaite, S.; Edström, K.; Hahlin, M. The cathode surface composition of a cycled Li–O$_2$ battery: A photoelectron spectroscopy study. *J. Phys. Chem. C* **2012**, *116*, 20673–20680.

[25] Chang, Z.; Qiao, Y.; Deng, H.; Yang, H. J.; He, P.; Zhou, H. S. A stable high-voltage lithium-ion battery realized by an in-built water scavenger. *Energy Environ. Sci.* **2020**, *13*, 1197–1204.

[26] Shao, Y. Y.; Ding, F.; Xiao, J.; Zhang, J.; Xu, W.; Park, S.; Zhang, J. G.; Wang, Y.; Liu, J. Making Li-air batteries rechargeable: Material challenges. *Adv. Funct. Mater.* **2013**, *23*, 987–1004.

[27] Zhang, X. Q.; Chen, X.; Hou, L. P.; Li, B. Q.; Cheng, X. B.; Huang, J. Q.; Zhang, Q. Regulating anions in the solvation sheath of lithium ions for stable lithium metal batteries. *ACS Energy Lett.* **2019**, *4*, 411–416.

[28] Xin, X.; Ito, K.; Dutta, A.; Kubo, Y. Dendrite-free epitaxial growth of lithium metal during charging in Li-O$_2$ batteries. *Angew. Chem., Int. Ed.* **2018**, *57*, 13206–13210.

[29] Sharon, D.; Hirsberg, D.; Salama, M.; Afri, M.; Frimer, A. A.; Noked, M.; Kwak, W.; Sun, Y. K.; Aurbach, D. Mechanistic role of Li$^+$ dissociation level in aprotic Li-O$_2$ battery. *ACS Appl. Mater. Interfaces* **2016**, *8*, 5300–5307.

[30] Burke, C. M.; Pande, V.; Khetan, A.; Viswanathan, V.; McCloskey, B. D. Enhancing electrochemical intermediate solvation through electrolyte anion selection to increase nonaqueous Li-O$_2$ battery capacity. *Proc. Natl. Acad. Sci. USA* **2015**, *112*, 9293–9298.

[31] Yoo, E.; Zhou, H. S. Enhanced cycle stability of rechargeable Li-O$_2$ batteries by the synergy effect of a LiF protective layer on the Li and DMTFA additive. *ACS Appl. Mater. Interfaces* **2017**, *9*, 21307–21313.

[32] Xu, J. J.; Liu, Q. C.; Yu, Y.; Wang, J.; Yan, J. M.; Zhang, X. B. *In situ* construction of stable tissue-directed/reinforced bifunctional separator/protection film on lithium anode for lithium-oxygen batteries. *Adv. Mater.* **2017**, *29*, 1606552.

[33] Chen, K.; Huang, G.; Ma, J. L.; Wang, J.; Yang, D. Y.; Yang, X. Y.; Yu, Y.; Zhang, X. B. The stabilization effect of CO$_2$ in lithium-oxygen/CO$_2$ batteries. *Angew. Chem., Int. Ed.* **2020**, *59*, 16661–16667.

[34] Frisch, M. J.; Trucks, G. W.; Schlegel, H. B.; Scuseria, G. E.; Robb, M. A.; Cheeseman, J. R.; Scalmani, G.; Barone, V.; Petersson, G. A.; Nakatsuji, H. et al. *Gaussian 09, Revision A.02*; Gaussian, Inc.: Wallingford CT, 2016.

[35] Becke, A. D. Density-functional exchange-energy approximation with correct asymptotic behavior. *Phys. Rev. A* **1988**, *38*, 3098–3100.

[36] Lee, C.; Yang, W. T.; Parr, R. G. Development of the Colle-Salvetti correlation-energy formula into a functional of the electron density. *Phys. Rev. B* **1988**, *37*, 785–789.

[37] Becke, A. D. A new mixing of Hartree-Fock and local density-functional theories. *J. Chem. Phys.* **1993**, *98*, 1372–1377.

[38] Marenich, A. V.; Cramer, C. J.; Truhlar, D. G. Universal solvation model based on solute electron density and on a continuum model of the solvent defined by the bulk dielectric constant and atomic surface tensions. *J. Phys. Chem. B* **2009**, *113*, 6378–6396.

[39] Meng, J. W.; Lei, M.; Lai, C. Z.; Wu, Q. P.; Liu, Y. Y.; Li, C. L. Lithium ion repulsion-enrichment synergism induced by core–shell ionic complexes to enable high-loading lithium metal batteries. *Angew. Chem., Int. Ed.* **2021**, *60*, 23256–23266.

[40] Qin, L.; Schkeryantz, L.; Zheng, J. F.; Xiao, N.; Wu, Y. Y. Superoxide-based K-O$_2$ batteries: Highly reversible oxygen redox solves challenges in air electrodes. *J. Am. Chem. Soc.* **2020**, *142*, 11629–11640.

[41] Younesi, R.; Hahlin, M.; Björefors, F.; Johansson, P.; Edström, K. Li-O$_2$ battery degradation by lithium peroxide (Li$_2$O$_2$): A model study. *Chem. Mater.* **2013**, *25*, 77–84.

[42] Lu, Y. C.; Crumlin, E. J.; Veith, G. M.; Harding, J. R.; Mutoro, E.; Baggetto, L.; Dudney, N. J.; Liu, Z.; Shao-Horn, Y. *In situ* ambientpressure X-ray photoelectron spectroscopy studies of lithium-oxygenredox reactions. *Sci. Rep.* **2012**, *2*, 715.

[43] Tułodziecki, M.; Leverick, G. M.; Amanchukwu, C. V.; Katayama, Y.; Kwabi, D. G.; Bardé, F.; Hammond, P. T.; Shao-Horn, Y. The role of iodide in the formation of lithium hydroxide in lithium-oxygen batteries. *Energy Environ. Sci.* **2017**, *10*, 1828–1842.

[44] Matsuda, S.; Kubo, Y.; Uosaki, K.; Nakanishi, S. Potassium ions

promote solution-route Li$_2$O$_2$ formation in the positive electrode reaction of Li-O$_2$ batteries. *J. Phys. Chem. Lett.* **2017**, *8*, 1142–1146.

[45] Zhao, S.; Wang, C. C.; Du, D. F.; Li, L.; Chou, S. L.; Li, F. J.; Chen, J. Bifunctional effects of cation additive on Na-O$_2$ batteries. *Angew. Chem., Int. Ed.* **2021**, *60*, 3205–3211.

[46] Ding, F.; Xu, W.; Graff, G. L.; Zhang, J.; Sushko, M. L.; Chen, X. L.; Shao, Y. Y.; Engelhard, M. H.; Nie, Z. M.; Xiao, J. et al. Dendrite-free lithium deposition via self-healing electrostatic shield mechanism. *J. Am. Chem. Soc.* **2013**, *135*, 4450–4456.

[47] Yang, Q. F.; Hu, J. L.; Meng, J. W.; Li, C. L. C-F-rich oil drop as a non-expendable fluid interface modifier with low surface energy to stabilize a Li metal anode. *Energy Environ. Sci.* **2021**, *14*, 3621–3631.

[48] Cong, G. T.; Wang, W. W.; Lai, N. C.; Liang, Z. J.; Lu, Y. C. A high-rate and long-life organic-oxygen battery. *Nat. Mater.* **2019**, *18*, 390–396.

[49] Zhang, X. P.; Sun, Y. Y.; Sun, Z.; Yang, C. S.; Zhang, T. Anode interfacial layer formation via reductive ethyl detaching of organic iodide in lithium-oxygen batteries. *Nat. Commun.* **2019**, *10*, 3543.

[50] Wu, X. H.; Niu, B.; Zhang, H. T.; Li, Z. G.; Luo, H. Y.; Tang, Y. L.; Yu, X. Y.; Huang, L.; He, X. R.; Wang, X. et al. Enhancing the reaction kinetics and reversibility of Li-O$_2$ batteries by multifunctional polymer additive. *Adv. Energy Mater.* **2023**, *13*, 2203089.

[51] Cai, Y. C.; Zhang, Q.; Lu, Y.; Hao, Z. M.; Ni, Y. X.; Chen, J. An ionic liquid electrolyte with enhanced Li$^+$ transport ability enables stable Li deposition for high-performance Li-O$_2$ batteries. *Angew. Chem., Int. Ed.* **2021**, *60*, 25973–25980.

[52] Tong, B.; Huang, J.; Zhou, Z. B.; Peng, Z. Q. The salt matters: Enhanced reversibility of Li-O$_2$ batteries with a Li[(CF$_3$SO$_2$)(n-C$_4$F$_9$SO$_2$)N]-based electrolyte. *Adv. Mater.* **2018**, *30*, 1704841.